The Effects of the Critical Ice Accretion on Airfoil and Wing Performance
NASA Contract #: NCC3-408

January 24, 1995 – November 30, 1996

Final Report
March 3, 1998

Michael S. Selig, Michael B. Bragg, and Farooq Saeed
University of Illinois at Urbana-Champaign
Department of Aeronautical and Astronautical Engineering

In support of the NASA Lewis Modern Airfoils Ice Accretion Test Program, the University of Illinois at Urbana-Champaign provided expertise in airfoil design and aerodynamic analysis to determine the aerodynamic effect of ice accretion on modern airfoil sections. The effort has concentrated on establishing a design/testing methodology for "hybrid airfoils" or "sub-scale airfoils," that is, airfoils having a full-scale leading edge together with a specially designed and foreshortened aft section. The basic approach of using a full-scale leading edge with a foreshortened aft section was considered to a limited extent over 40 years ago. However, it was believed that the range of application of the method had not been fully exploited. Thus a systematic study was being undertaken to investigate and explore the range of application of the method so as to determine its overall potential.

The approach proved successful as detailed in the attached appendices:

A. Initial paper documenting the approach:

> Saeed, F., Selig, M.S. and Bragg, M.B., "A Design Procedure for Subscale Airfoils with Full-Scale Leading Edges for Ice Accretion Testing," AIAA 34th Aerospace Sciences Meeting, AIAA Paper 96-0635, Reno, NV, January 1996. Also appears as Saeed, F., Selig, M.S., and Bragg, M.B., "A Design Procedure for Subscale Airfoils with Full-Scale Leading-Edges for Ice Accretion Testing," *Journal of Aircraft*, Vol. 34, No. 1, January–February 1997, pp. 94–100.

B. An extension of the method that allows for satisfying full-scale ice accrections on sub-scale airfoils over a range of angles of attack:

> Saeed, F., Selig, M.S., and Bragg, M.B., "A Hybrid Airfoil Design Method to Simulate Full-Scale Ice Accretion throughout a Given C_l-Range," AIAA 35th Aerospace Sciences Meeting, AIAA Paper 97-0054, Reno, NV, January 1997. To appear as Saeed, F., Selig, M.S., and Bragg, M.B., "A Hybrid Airfoil Design Method to Simulate Full-Scale Ice Accretion throughout a Given α-Range," *Journal of Aircraft*.

Related research dealing with using subscale models with full-scale leading edges for ice accretion is continuing under NASA Cooperative Agreement Award # NCC3-509.

AIAA 96-0635

A Design Procedure for Subscale Airfoils with Full-Scale Leading-Edges for Ice Accretion Testing

Farooq Saeed, Michael S. Selig and Michael B. Bragg
University of Illinois at Urbana-Champaign
Urbana, IL

34th Aerospace Sciences Meeting & Exhibit
January 15-18, 1996 / Reno, NV

A DESIGN PROCEDURE FOR SUBSCALE AIRFOILS WITH FULL-SCALE LEADING EDGES FOR ICE ACCRETION TESTING

Farooq Saeed,* Michael S. Selig† and Michael B. Bragg‡
Department of Aeronautical and Astronautical Engineering
University of Illinois at Urbana-Champaign
Urbana, Illinois 61801

ABSTRACT

A design procedure for subscale airfoils with full-scale leading edges that exhibit full-scale water droplet impingement characteristics in an incompressible, inviscid flow is presented. The design procedure uses validated airfoil design, flow analysis and water droplet impingement simulation codes to accomplish the task. To identify and isolate important design variables in the design, numerous trade studies were performed. The paper presents the results of the trade studies and briefly discusses the role of important design variables in the subscale airfoil design. The effect of these design variables on circulation, velocity distribution and impingement characteristics is discussed along with the accompanying implications and compromises in the design. A strategy to incorporate viscous effects into the design is also presented. The paper also presents the design of a half-scale airfoil model with a 5% upper and 20% lower full-scale surface of the Learjet 305 airfoil leading-edge and compares its aerodynamic as well as the droplet impingement characteristics with that of the Learjet 305 airfoil.

NOMENCLATURE

c = airfoil chord length
C_d = airfoil drag coefficient
C_l = airfoil lift coefficient
c_{mo} = airfoil pitching moment coefficient
F_r = Froude number, $U/\sqrt{cg}$
K = droplet inertia parameter, $\rho_w \delta^2 U/18c\mu$
K_S = trailing-edge thickness parameter
M = freestream Mach number
Re = freestream Reynolds number, $\rho U c/\mu$
R_U = droplet freestream Reynolds number, $\rho \delta U/\mu$
S = airfoil surface arc length measured from the leading-edge

T = freestream static temperature
u, v = local flowfield horizontal and vertical velocity components
U = freestream velocity
V = surface velocity
VMD = volume median droplet diameter
x, y = airfoil coordinates
x_o, y_o = initial horizontal and vertical displacement of the droplet
$x_m, \bar{x}_m$ = upper and lower surface match locations
$x_r, \bar{x}_r$ = upper and lower surface pressure recovery locations
v_1 = design velocity level for segment 1
α = angle of attack relative to the chord line
α_e = effective angle of attack relative to the nose section chord line, $\alpha - \gamma$
$\alpha^*, \bar{\alpha}^*$ = upper and lower surface multipoint design angle of attack distribution
β = local impingement efficiency
ϕ_{le} = leading-edge arc limit
γ = nose droop angle
Γ = circulation strength normalized by Uc
$\bar{\Gamma}$ = circulation strength, m^2/s
δ = droplet diameter
η = normalized subscale airfoil chord length, c_{ss}/c_{fs}
μ = air viscosity
ρ = air density
ρ_w = water density
τ = finite trailing-edge angle

Subscripts:
fs = full-scale airfoil
i = inviscid
l = lower surface
ss = subscale airfoil
u = upper surface
v = viscous

* Graduate Research Assistant. Student Member AIAA.
† Assistant Professor. Member AIAA.
‡ Professor. Associate Fellow AIAA.

INTRODUCTION

Recent aircraft accidents have raised important flight safety issues related to the effect of ice accretion on airfoil and wing performance. In order to improve flight safety, a better understanding of the effect of ice accretion on the aerodynamic performance of modern airfoils is required. One important step in this process is to evaluate the aerodynamic performance of the airfoil sections (or the wing as a

whole) at the icing conditions within the certification icing envelop that result in the largest performance penalties.

Since ice accretion scaling is still not well understood, testing at full-scale or near full-scale conditions is highly desirable. The available ice accretion tunnels, however, are too small to test full-scale airfoils or wings of most aircraft of interest. Numerous investigators have performed experimental or analytical studies[1-4] in an effort to evaluate full-scale icing protection systems for wing sections using truncated airfoil models. These truncated airfoil models utilize a full-scale leading edge section followed by a faired or flapped aft section that, in effect, reduces the overall length or chord of the model. To our knowledge, however, no systematic study has been performed to provide insight into the design of the aft section.

With these issues in mind, a subscale model design procedure was formulated with the objective of providing design guidance for subscale models that simulate full-scale water droplet impingement characteristics. It is assumed that ice accretion will be the same if droplet impingement, surface geometry and surface flowfield are the same provided the same cloud properties, model surface quality, model surface thermodynamic characteristics exist. Using the fact that ice usually accretes only on the airfoil leading edge, where the supercooled water droplets impinge and form ice, the subscale airfoil model is designed with a leading-edge geometry (first 10-20% of chord) identical to that of the full-scale leading edge. The design of the aft section is such that it provides full-scale flowfield and droplet impingement on the leading edge. Using this formulation, the effect of various design variables on the inviscid flowfield and droplet impingement characteristics of the subscale airfoil was examined to obtain useful guidelines for the design. The final design is based on viscous considerations as well.

The model design procedure for full-scale flowfield and droplet impingement simulation uses validated computational airfoil aerodynamics and droplet impingement codes,[5-15] specifically, an inverse design method,[10] the Eppler code,[8,9] XFOIL[11] and AIRDROP.[12]

DESIGN APPROACH

A conceptual illustration of the subscale airfoil design procedure is shown in Fig. 1. First, a droplet impingement code can be used to predict the limits of the droplet impingement, which defines the initial ice accretion envelop. (The droplet impingement code, AIRDROP,[12] is discussed later.) Once
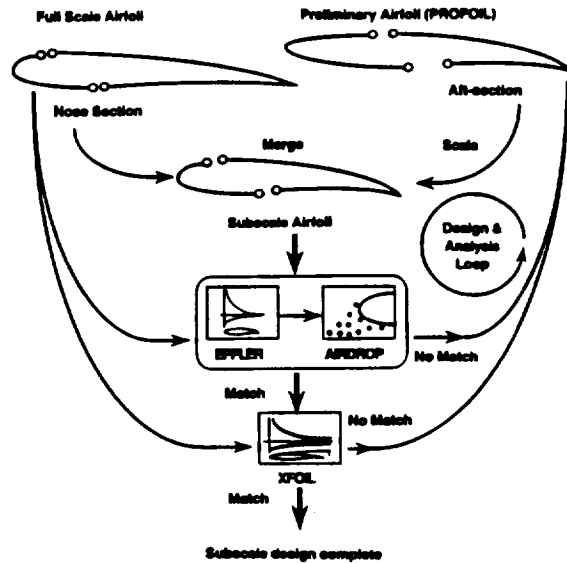

Fig. 1 A conceptual illustration of the subscale airfoil design procedure.

the limits of impingement are known over the leading edge of the full-scale airfoil, that part of the full-scale airfoil geometry is fixed for the subsequent subscale airfoil shapes. For the sake of discussion, this fixed leading-edge section, which is common to both the full scale airfoil and the subscale airfoil, is referred to as the nose section while the remaining section of the subscale airfoil profile is referred to as the aft section. The aft section of the subscale airfoil is then designed to provide full-scale flowfield and droplet impingement on the nose section of the subscale airfoil.

An initial geometry for the aft section is obtained through the use of a multipoint inverse airfoil design code[10] (PROFOIL). The design of this intermediate airfoil, from which the aft section of the subscale airfoil is derived, is governed by several constraints, namely, the scale of the subscale airfoil, the upper and lower surface thickness and slope at the junction between the nose and aft sections $(x_m, \bar{x}_m)$, and a desired form for the pressure recovery characteristics. Apart from these constraints, additional continuity and closure constraints that form an integral part of the inverse design methodology[10] are also satisfied in order to achieve a physically possible design. A multi-dimensional Newton iteration scheme is employed to satisfy these constraints. The dependent and independent Newton variables[10] used in the design are listed Table 1. Once the constraints are satisfied, the aft section is combined with the nose section to form a subscale airfoil.

The potential flow over both the subscale and the full-scale airfoils is then analyzed using the

Table 1 Newton variables used in the design.

Dependent Variables	Independent Variables
$K_S = 0.3$	ϕ_{le}
c_{mo}	v_1
$y(x_m)$	α^*
$y(\overline{x}_m)$	$\overline{\alpha}^*$

Eppler code, which has the capability to analyze the potential flow over the airfoils using a method that employs panels with distributed surface singularities. The singularities used are vorticities distributed parabolically along each panel. Results predicted by the Eppler code have been shown to compare well with experiments.[16,17]

In order to have a physically similar flow in the vicinity of the nose section of both the subscale and the full-scale airfoils, the analysis is performed at the same angle of attack relative to the nose section chord of both the airfoils. The local inviscid velocity distributions over the nose section and the stagnation point locations on both the subscale and full-scale airfoils are then compared. If the desired velocity distribution over the nose section and stagnation point location are not achieved, the aft section of the subscale airfoil is redesigned and again merged with the nose section to form a new subscale airfoil. The flow over the new subscale airfoil is then analyzed and compared with that over the full scale airfoil. The process is repeated until the desired inviscid velocity distribution over the nose section and the stagnation point location are achieved.

In the next step, the subscale airfoil circulation, water droplet trajectories and water droplet impingement characteristics are determined from AIRDROP. The airfoil droplet impingement code, AIRDROP, written by Bragg[12] predicts droplet trajectories and the resultant impingement efficiency on single element airfoils in incompressible flow. The code has been validated against NACA airfoil droplet impingement data and compares well when the cloud droplet size distribution is modeled correctly and the code is run matching the airfoil lift coefficient.[12] Comparisons with predicted and measured rime ice accretion show good agreement.

The numerical procedure employed by AIRDROP consists of two steps. First, the flowfield around the airfoil is determined by Woan's method.[18] Second, single water droplet trajectories are calculated from the trajectory equation,[12] which in nondimensional form contains the three additional similarity parameters R_U, F_r and K, apart from Re and M. Thus, given R_U, F_r, K, the droplet initial location, and the airfoil geometry, single water droplet trajectories are

determined from the trajectory equation.[12]

The individual droplet trajectories are combined to calculate the local impingement efficiency β (= dy_o/dS). The impingement efficiency represents the dimensionless mass flux of impinging droplets at a point on the airfoil. Here, y_o is the initial y displacement of an impinging droplet far ahead ($x_o = -5c_{fs}$) of the airfoil, and S is the surface length of the impact location measured from the leading edge of the airfoil. The AIRDROP code calculates a series of droplet trajectories, fits a cubic spline through the y_o vs S data points of the impinging droplets, and then computes the slope of the spline at a series of surface positions. This slope is β at that surface location. In this paper, the y_o vs S plot is referred to as the y_o-curve and the β vs S plot is referred to as the β-curve. And the term "impingement characteristics" refers to both the y_o-curve and β-curve.

The impingement characteristics of both the full scale and subscale airfoil are then compared with each other. If the agreement in the impingement characteristics is poor, the subscale airfoil is modified and the design process is repeated again until a good agreement is reached.

As will be shown later, the amount of circulation plays a dominant role in determining the impingement characteristics through its impact on the flowfield droplet trajectories (y_o-curve). The expression for the total circulation can be derived from the relation

$$L = \rho U \overline{\Gamma} = \frac{1}{2}\rho U^2 c C_l \qquad (1)$$

which yields

$$\Gamma = \frac{\overline{\Gamma}}{Uc} = \frac{1}{2}C_l \qquad (2)$$

Therefore, the full-scale and subscale airfoil circulation is,

$$\Gamma_{fs} = \frac{1}{2}C_{l,fs}, \qquad \Gamma_{ss} = \frac{\eta}{2}C_{l,ss} \qquad (3,4)$$

respectively, where η is the normalized subscale airfoil chord length.

Finally, in order to obtain a physically realistic subscale airfoil design, consideration must also be given to viscous and compressibility effects to determine the true merits of the design. A discussion of the viscous considerations is presented in a later section.

IMPLEMENTATION

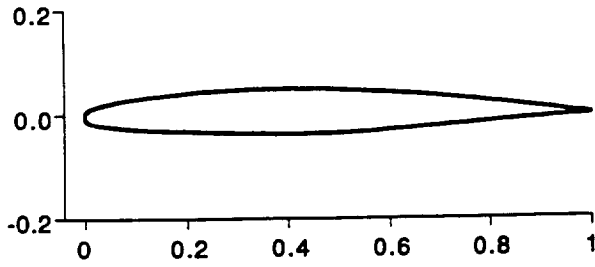To expedite the design procedure, the Eppler code, PROFOIL, and AIRDROP were integrated

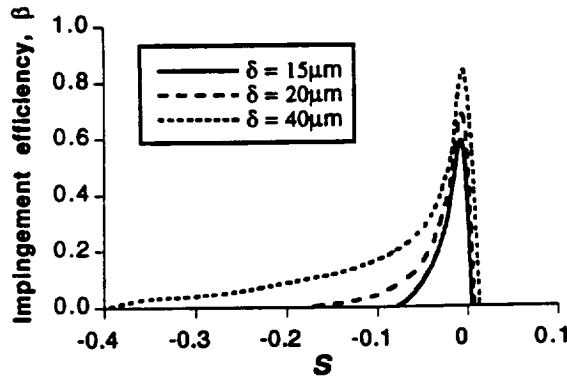**Fig. 2 The Learjet 305 (GLC 305) airfoil.**

Fig. 3 Droplet impingement efficiency predicted by AIRDROP for the Learjet 305 airfoil.

into a single computer program. Then, the constraints on the subscale airfoil design were defined in terms of the fixed nose section geometry, velocity distribution over the nose section, total circulation and the angle of attack relative to the nose section of a full-scale airfoil. In order to satisfy all of the above constraints, numerous parametric trade studies were performed to help identify and isolate various key independent design variables. These independent variables were later identified as the pitching moment coefficient c_{mo} of the airfoil from which the aft section of the subscale airfoil is derived, the scale η of the subscale airfoil, the nose droop angle γ, and the upper and lower surface pressure recovery locations x_r and $\bar{x}_r$.

To illustrate the effects of the independent design variables on the subscale airfoil design, the Learjet 305 (GLC 305) airfoil, shown in Fig. 2, was selected as the full-scale airfoil along with the flight and icing conditions listed in Table 2. At these conditions for the GLC 305 airfoil, AIRDROP predicts a lift coefficient $C_{l,fs} = 0.736$ and the circulation $\Gamma_{fs} = 0.368$. Figure 3 shows the corresponding β-curves as predicted by AIRDROP. For $VMD = 20\mu m$, AIRDROP predicts the maximum limits of impingement as $S_u = 0.0076 \, (x/c = 0.0019)$ on the upper surface and $S_l = -0.1822 \, (x/c = 0.1738)$ on the lower surface.

Table 2 Typical Flight and Icing conditions.

Airspeed, U	$= 87$ m/s (175 kt)
Static temperature, T	$= -5$ deg C
Reynolds number, Re	$= 6 \times 10^6$
Mach number, M	$= 0.28$
VMD	$= 15\text{--}40\mu m$
Angle of attack, α	$= 6$ deg

Since the limits of impingement define the surface within which ice will accrete on the airfoil, only that part of the full scale geometry need be fixed as the nose section for the subscale airfoil. The nose section size is kept to a minimum, thereby, allowing more flexibility in the design of the aft section to satisfy the constraints. Thus, the nose section geometry was selected as the full scale airfoil surface from $x/c = 0.05$ on the upper surface to $x/c = 0.20$ on the lower surface. Moreover, a half-scale ($\eta = 0.5$) subscale model was selected as the baseline case. Based on the size of droplets under consideration, the effect of gravity on the droplets was considered negligible and, therefore, was ignored.

Most of the important effects can be examined by only considering inviscid effects; that is, boundary-layer displacement effects are second order relative to the effects of pitching moment, subscale airfoil chord length and the nose droop. Thus the remainder of this section is divided into inviscid and viscous considerations.

Inviscid Considerations
Effect of Pitching Moment Coefficient (c_{mo})

The effect of the pitching moment coefficient is illustrated in Fig. 4, in which, an increase in the pitching moment coefficient c_{mo} (more negative) results in a subscale airfoil with a greater aft camber and, therefore, a higher aft loading as well as an increase in the amount of circulation. The change in circulation with c_{mo} is found to be nearly linear. The droplet impingement characteristics, specifically the y_o-curves, also indicate a strong dependence on the value of circulation which makes the pitching moment coefficient c_{mo} the main independent design variable (Note that, c_{mo} assumes a role of a dependent design variable in the design of the aft section). Figure 4(d) indicates that the subscale airfoil requires slightly less circulation (by 4.5%) than the full scale airfoil to achieve full-scale droplet impingement. One explanation is that the subscale airfoil is able to achieve full-scale droplet impingement with slightly less circulation due to the distribution of vorticity. In the case of a subscale airfoil the vorticity is more "concentrated" near the leading-edge than in the case of the full scale airfoil resulting in
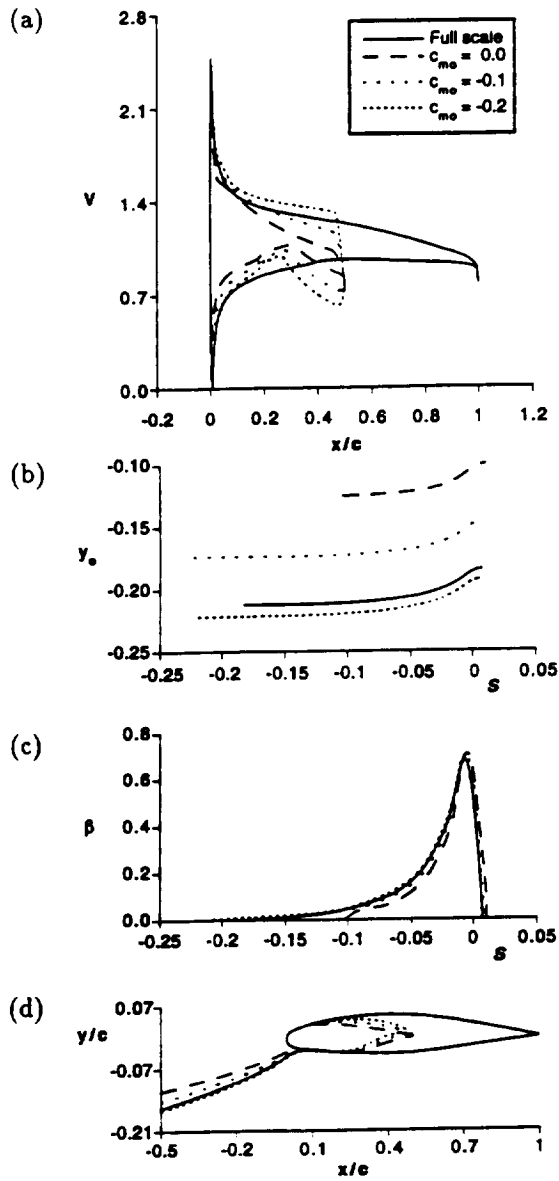
Fig. 4 The effect of pitching moment coefficient on (a) the velocity distribution, (b) initial displacement, (c) droplet impingement efficiency and (d) the tangent droplet trajectories.
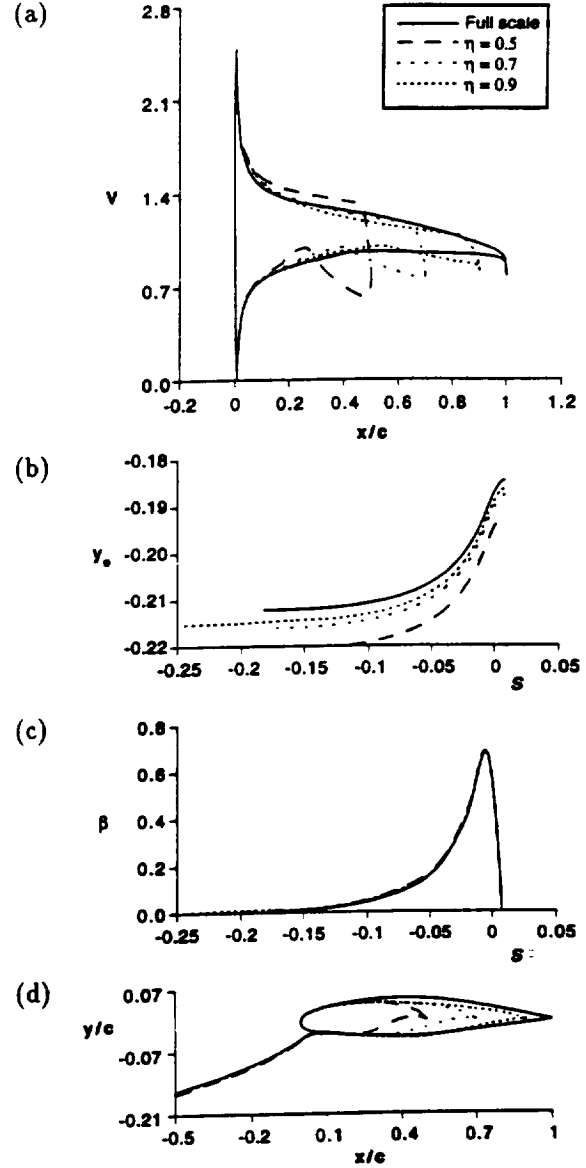
Fig. 5 The effect of chord length on (a) the velocity distribution, (b) initial displacement, (c) droplet impingement efficiency and (d) the tangent droplet trajectories.

a greater upwash in close proximity of the airfoil. Thus a lower value of overall circulation is required to simulate full scale droplet impingement.

Effect of Chord Length (η)

To examine the effect of normalized subscale chord length η on the design, subscale airfoils were designed for three different values of η, that is, 0.5, 0.7 and 0.9. Initially, the three subscale airfoils were designed such that they produced the same amount of circulation as the full scale airfoil. Figure

5 shows the resulting velocity distribution impingement characteristics and the airfoil shapes. The results indicate that as the scale of the subscale model is reduced, the aft-loading on the airfoil increases significantly in order for it to produce the same amount of circulation. The mismatch in the y_o-curves, Fig. 5(b), suggests that subscale models require less circulation to achieve full scale impingement characteristics. Moreover, the results also suggest that the smaller the scale, the less circulation required to simulate full scale droplet impingement
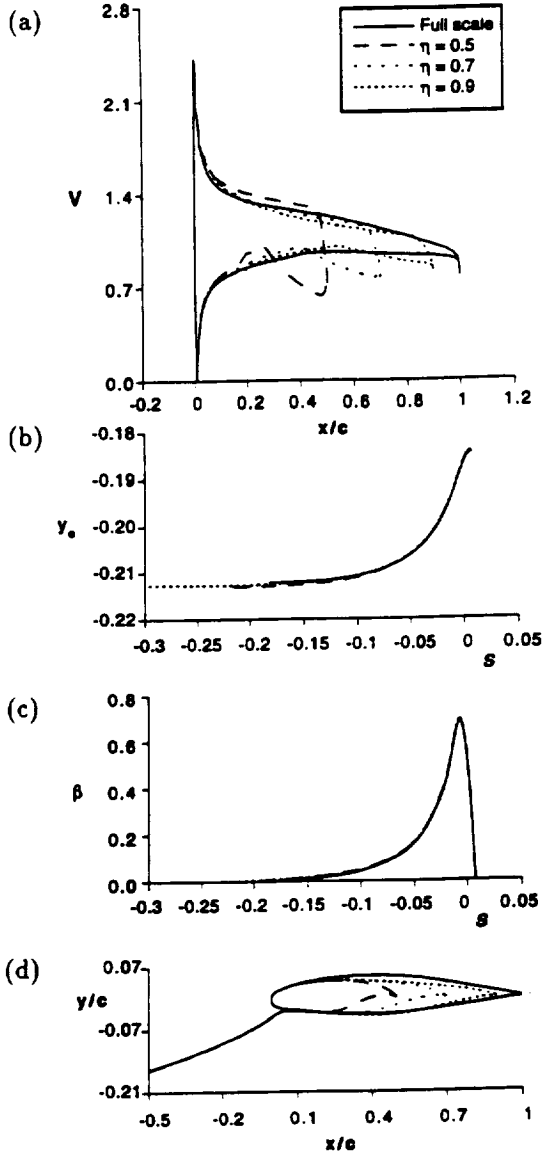
5

(a)

(b)

(c)

(d)

Fig. 6 Results showing (a) the velocity distribution, (b) initial displacement, (c) droplet impingement efficiency and (d) the tangent droplet trajectories at the matched conditions.
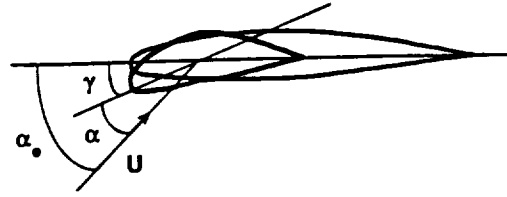

Fig. 7 The nose droop angle.
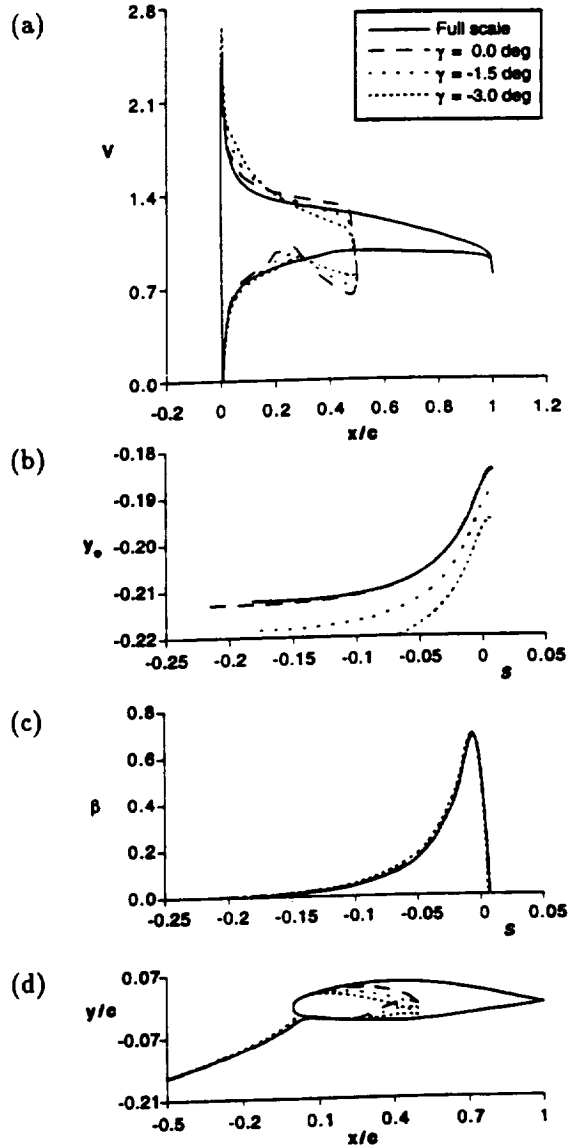
(a)

(b)

(c)

(d)

Fig. 8 The effect of nose droop on (a) the velocity distribution, (b) initial displacement, (c) droplet impingement efficiency and (d) the tangent droplet trajectories.

characteristics. The subscale airfoils shown in Fig. 6 were designed such that the impingement characteristics, specifically, the y_o-curves were matched. The match in y_o-curves was achieved by designing subscale airfoils with reduced circulation as compared with the ones in Fig. 5. The results also indicate that the amount of circulation required to simulate full scale droplet impingement vary from $(0.955\Gamma_{fs})$ for η of 0.5 to $(0.983\Gamma_{fs})$ for η of 0.9.

Effect of Nose Droop Angle (γ)

The effect of the nose droop angle γ, shown in Fig. 7, becomes obvious from Fig. 8 which illustrates

the usefulness of the nose droop in reducing the high aft-loading on airfoils. In order to keep the angle of attack relative to the nose section chord constant

for both the full scale and subscale airfoils, the subscale airfoil with a nose droop is analyzed at an effective angle of attack α_e which takes into account the nose droop angle. As a result, the subscale airfoils with nose sections droop downwards are analyzed at higher angles of attack than those without the nose droop. Figure 8 shows the results of the subscale airfoil design with different nose droop angles for the same value of circulation as that of the half-scale model without the nose droop. The results indicate that the nose droop results in an increase in the camber of the subscale airfoil and, therefore, the subscale airfoil circulation. Moreover, the subscale airfoils with the nose drooped downwards also operate at higher absolute angles of attack defined by α_e. As a result of this increase, the impingement characteristics show a mismatch. By decreasing the amount of circulation by an appropriate amount, the mismatch was removed as shown in Fig. 9. The reduction in the value of circulation as compared with that for the full scale airfoil varies from $(0.955\Gamma_{fs})$ for γ of 0 deg to $(0.892\Gamma_{fs})$ for γ of -3 deg.

Other Effects

The upper and lower surface pressure recovery locations x_r and $\overline{x}_r$ (see Fig. 10) control to a great extent the shape of the airfoil near its trailing edge. Although, the effect of moving the pressure recovery locations x_r and $\overline{x}_r$ results in a significant amount of improvement in the velocity distributions and ultimately the viscous characteristics, the change in the droplet impingement characteristics is, however, small.

The above study, based on inviscid considerations alone, illustrates the effect of different independent design variables on the subscale airfoil design. The results indicate that subscale airfoils require less circulation to simulate full scale airfoil droplet impingement characteristics. The pitching moment coefficient c_{mo} can be used effectively to achieve the desired amount of circulation. Since subscale airfoils tend toward high aft-loading in order to simulate the desired impingement characteristics, a nose droop can be used effectively to offset the high aft-loading to a large extent. The above study also reveals that subscale airfoils with a nose droop require even less circulation to achieve the desired impingement characteristics. Moreover, a subscale airfoil with a nose droop (downwards) must operate at a higher absolute angle of attack to simulate full scale impingement characteristics over its nose section. Operation at high absolute angles of attack makes the subscale airfoil highly susceptible to flow separation and, therefore, it becomes necessary to evaluate the performance by means of a viscous analysis of the
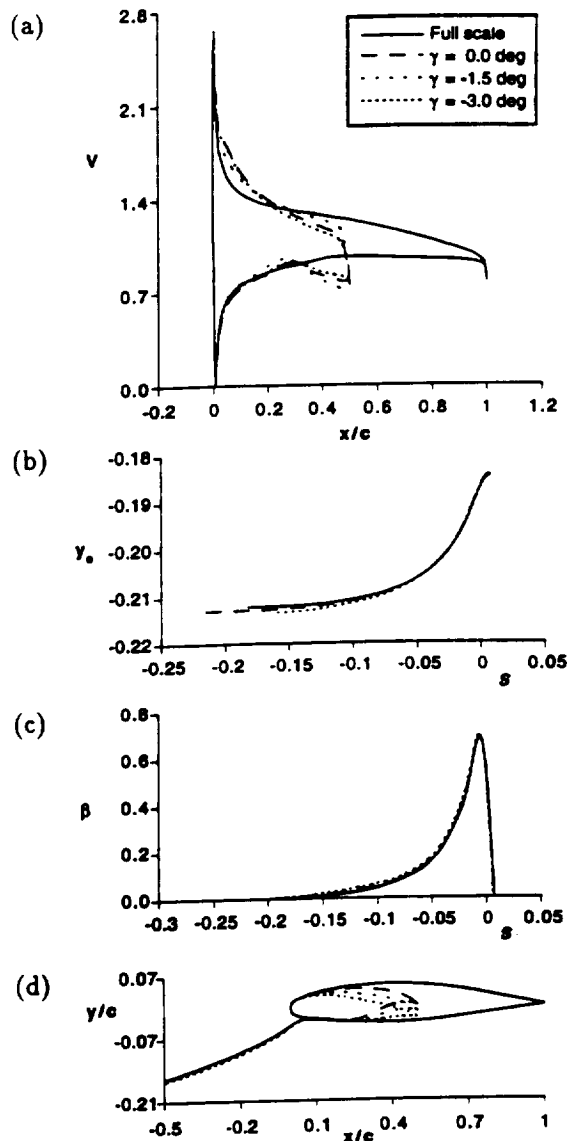

Fig. 9 Results showing (a) the velocity distribution, (b) initial displacement, (c) droplet impingement efficiency and (d) the tangent droplet trajectories at the matched conditions.

flowfield over the subscale airfoil at the design conditions.

Viscous Considerations

To determine the true merits of the design, a viscous flowfield analysis must form an essential part of the design. For the purpose of viscous flowfield analysis, XFOIL was utilized. XFOIL is a modified version of the ISES code[19] which has been successfully applied to the design and analysis of airfoils for various applications varying from human-powered aircraft[20] to high Reynolds number transonic transport. XFOIL utilizes a fully compatible laminar and
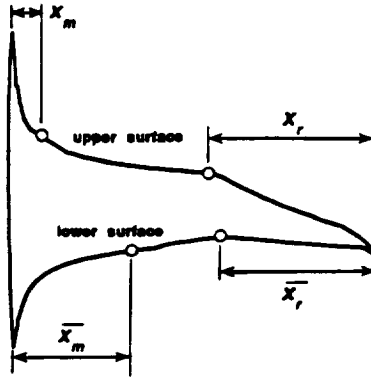
Fig. 10 The upper and lower surface match and pressure recovery locations.

Table 3 Design Flight and Icing conditions.

Variable	Full scale	Subscale
U, m/s	87	87
T, deg C	−5	−5
Re	6×10^6	3×10^6
M	0.28	0.28
c, m	1.0	0.5
VMD, μm	20	20
α, deg	6	6
γ, deg	0	−3
α_e, deg	6	9

Table 4 The converged solution.

Dependent Variables	Independent Variables
$K_S = 0.3$	$\phi_{le} = 189.53$ deg
$c_{mo} = -0.065$	$v_1 = 2.133$
$y(x_m = 0.05)$	$\alpha^* = 8.93, 11.93, 14.93$ deg
$y(\bar{x}_m = 0.20)$	$\bar{\alpha}^* = 1.17$ deg (all segments)
$\tau = 6$ deg	$x_r = 0.0114c$ $\bar{x}_r = 0.4746c$

turbulent viscous formulation, a reliable transition formulation and a global Newton iteration method to converge onto a flowfield solution.

The viscous analysis was performed to determine the effect of the presence of the viscous boundary on the flowfield. Typically inviscid flowfield codes over predict the airfoil lift-curve slope and the lift on an airfoil as compared to viscous flowfield codes since, in a viscous flowfield, the presence of boundary-layer decambers the airfoil and, therefore, reduces the C_l. This results in an error in the droplet trajectory calculation since at the design angle of attack, the inviscid flowfield is for a higher lift coefficient, and therefore, greater circulation. To account for this effect, a procedure called the "Matched Lift Coefficient Method" is employed, in which, the inviscid flowfield is analyzed at matched lift coefficient instead of matched angle of attack with the viscous flowfield. A brief outline of this procedure as applied to the subscale airfoil design is as follows.

Initially, the viscous $C_{l,fs}$ is determined at the design angle of attack with the help of XFOIL. Using $C_{l,fs}$, an angle of attack $\alpha_{i,fs}$ is found such that running the inviscid flowfield code at $\alpha_{i,fs}$ produces an inviscid C_l which matches $C_{l,fs}$, the viscous C_l. Next, the inviscid flowfield as well as the droplet impingement characteristics of the full scale airfoil are determined at $\alpha_{i,fs}$ and set as the target for the subscale airfoil design. A subscale airfoil is then designed to match the target flowfield and impingement characteristics. Once a match is achieved, a viscous analysis of the subscale airfoil is performed at the matched conditions to determine the viscous $C_{l,ss}$. As in the full scale airfoil case, an inviscid $\alpha_{i,ss}$ is calculated and is used to determine the inviscid flowfield and droplet impingement characteristics for comparison with the target flowfield and droplet impingement characteristics. If the desired charac-

teristics are achieved, the design is complete, otherwise, the subscale airfoil is modified and the whole process is repeated again until the desired match is achieved.

A DESIGN EXAMPLE

In this section, a specific design example is presented with the objective to design a half-scale model of the GLC 305 airfoil that simulates full scale droplet impingement. Table 3 lists the flight and icing conditions for the final design, whereas, Table 4 lists the final values of the design variables for the converged solution. The subscale airfoil was designed with a finite trailing-edge angle $\tau = 6$ deg. The effects due to compressibility were also considered during the viscous flow analysis of both the airfoils.

Fig. 11 shows the comparison between the inviscid velocity distributions for the converged solution at $\alpha_e = 6$ deg. Fig. 12 shows the comparison between the velocity distributions (viscous) at the design conditions, where, $C_{l,fs} = 0.7690$ and $C_{l,ss} = 0.6074$. The respective inviscid velocity distributions for the matched lift coefficient case are shown in Fig. 13(a). All the figures show good agreement in velocity distribution over the common nose section. The comparison of the impingement characteristics corresponding to the respective matched lift coefficient cases is shown in Fig. 13(b) and (c), whereas, a comparison of tangent droplet trajectories is shown in Fig. 13(d). The results indicate excellent agreement in impingement efficiency. The tangent droplet trajectories, although originating at
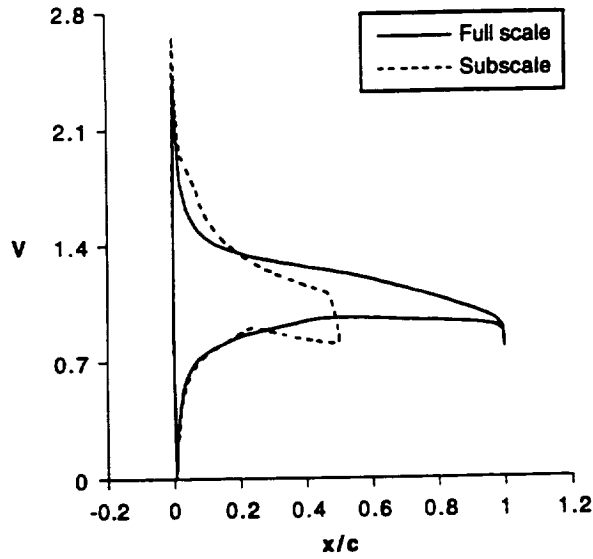
8

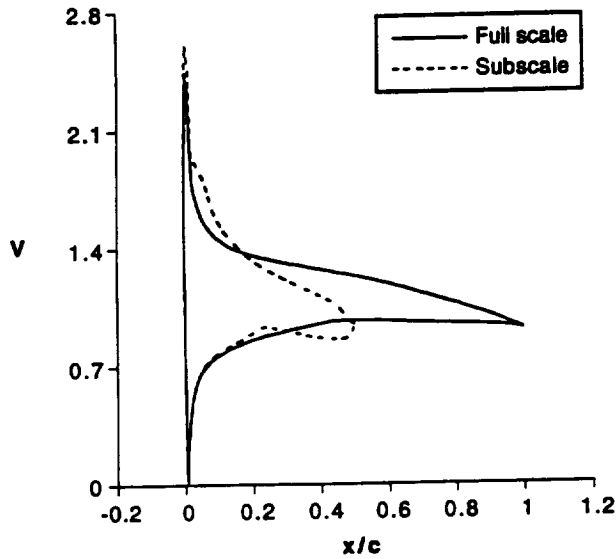Fig. 11 Comparison between the inviscid velocity distribution at $\alpha_e = 6$ deg.

Fig. 12 Comparison between the velocity distribution at the design conditions listed in Table 3.
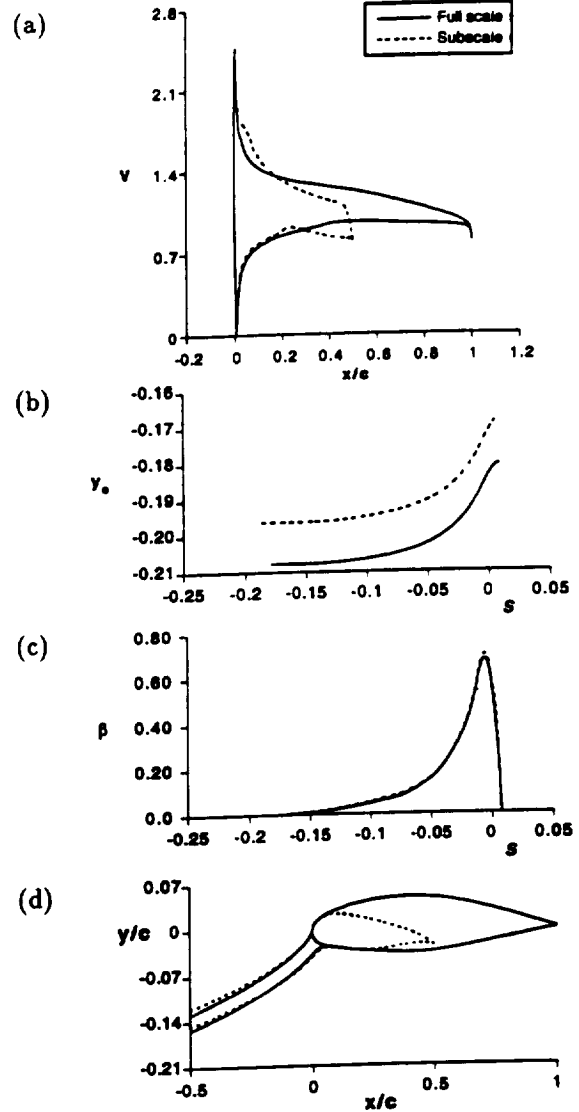

Fig. 13 Comparison between (a) the velocity distribution, (b) the initial displacement, (c) droplet impingement efficiency and (d) the tangent droplet trajectories at $\alpha_{i,fs}$ and $\alpha_{i,ss}$, corresponding to the respective matched lift coefficients.

different locations along the y-axis, are matched in the vicinity of the leading-edge. This is consistent with the observations made during the case studies that subscale airfoils require a lower value of circulation to achieve full scale droplet impingement characteristics.

CONCLUSIONS

Several important conclusions can be drawn from this study. First, it is shown that subscale airfoils with full-scale leading edges can be designed to exhibit full-scale droplet impingement and, there-

fore, ice accretion. Second, the results indicate that subscale airfoils require less circulation to simulate full scale airfoil droplet impingement characteristics. The pitching moment coefficient, of the airfoil from which the aft section for the subscale airfoil is derived, can be used effectively to achieve the desired amount of circulation on the subscale airfoil. Third, since subscale airfoils tend toward high aft-loading in order to simulate the desired droplet impingement characteristics, a nose droop can be used effectively to offset the high aft-loading. Fourth, an airfoil with
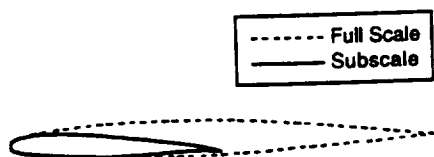
Fig. 14 The final subscale airfoil and the Learjet 305 airfoil.

a nose droop (downwards) must operate at a higher absolute angle of attack in order to keep the same angle of attack relative to its nose section as the full scale airfoil to simulate full scale impingement characteristics. Operation at high absolute angles of attack makes the subscale airfoil highly susceptible to flow separation and, therefore, it becomes necessary to integrate the viscous analysis of the flowfield over the subscale airfoil into the design process. Fifth, to incorporate viscous and compressibility effects, the "matched lift coefficient method" outlined in the paper was applied successfully in the final design example.

Although, the design method outlined in this paper is only limited to a point design, the method can be extented to a multipoint design similar in lines to the existing multipoint inverse airfoil design methods by integrating viscous boundary-layer equations and the droplet trajectory equation with the inverse airfoil design method.

ACKNOWLEDGMENTS

REFERENCES

[1]Hauger, H.H., and Englar, K.G. "Analysis of Model Testing in an Icing Wind Tunnel," Rep. No. SM 14993, Douglas Aircraft Co., Inc., May 14, 1954.

[2]Sibley, P.J., and Smith, R.E., Jr. "Model Testing in an Icing Wind Tunnel," Rep. No. LR 10981, Lockheed Aircraft Cor., Inc., Oct. 14, 1955.

[3]Langmuir, I., and Blodgett, K., "A Mathematical Investigation of Water Droplet Trajectories," Army Air Forces TR 5418, Feb. 1946.

[4]Glahn, U. H. von, "Use of Truncated Flapped Airfoils for Impingement and Icing Tests of Full-Scale Leading-Edge Sections," NACA RM E56E11, July 1956.

[5]Soinne, E. and Laine, S., "An Inverse Boundary Element Method for Single Component Airfoil Design," Journal of Aircraft, Vol. 22, No. 6, June 1985, pp. 541-543.

[6]Ormsbee, I.A. and Chen, A.W., "Multiple element Airfoils Optimized for Maximum Lift Coefficient," AIAA Journal, Vol. 10, No. 12, December 1972, pp. 1620-1624.

[7]Kennedy, J.L. and Marsden, D.J., "A Potential Flow Design Method for Multicomponent Airfoil Sections," Journal of Aircraft, Vol. 15, No. 1, January 1978, pp. 47-52.

[8]Eppler, R., "Direct Calculation of Airfoils from Pressure Distribution," NASA TT F-15, 417, March 1974. (Translated from Ingenieur-Archive, Vol.25, No.1, 1957, pp. 32-57)

[9]Eppler, R., Airfoil Design and Data, Springer-Verlag, New York, 1990.

[10]Selig, M.S. and Maughmer, M.D., "A Multipoint Inverse Airfoil Design Method Based on Conformal Mapping," AIAA Journal, Vol. 30, No. 5, 1992, pp. 1162-1170.

[11]Drela, M., "XFOIL: An Analysis and Design System for Low Reynolds Number Airfoils." Proceedings of the Conference on Low Reynolds Number Aerodynamics, Norte Dame, Indiana, June 1989. In Lecture Notes in Engineering, No. 54, Springer-Verlag, New York, pp. 1-12.

[12]Bragg, M.B., "Rime Ice Accretion and Its Effect on Airfoil Performance," Ph. D. Dissertation, The Ohio State University, Columbus, Ohio, 1981.

[13]Bragg, M.B., "The Effect of Geometry on Airfoil Icing Characteristics," Journal of Aircraft, Vol. 21, No. 7, July 1984, pp. 505-511.

[14]Bragg, M.B., "A Similarity Analysis of the Droplet Trajectory Equation," AIAA Journal, Vol. 20, No. 12, Dec. 1982, pp. 1681-1686.

[15]Ruff, A.G. and Berkowitz, "User's Manual for the NASA Lewis Ice Accretion Prediction Code (LEWICE)," NASA CR 185129, 1990.

[16]Somers, D.M., "Design and Experimental Results for a Flapped Natural-Laminar-Flow Airfoil for General Aviation Application," NASA TP-1865, June 1981.

[17]Maughmer, M.D., and Somers, D.M., "Design and Experimental Results for a High-Altitude, Long Endurance Airfoil," Journal of Aircraft, Vol. 26, No. 2, Dec. 1989, pp. 148-153.

[18]Woan, C.J., "Fortran Programs for Calculating the Incompressible Potential Flow About a Single

Element Airfoil Using Conformal Mapping," The Ohio State University, Aeronautical and Astronautical Research Laboratory, TR AARL 80-02, Columbus, Ohio, January 1980.

[19]Drela, M., and Giles, M.B., *"ISES: A Two-Dimensional Viscous Aerodynamic Design and Analysis Code,"* AIAA 87-0424, Jan. 1987.

[20]Drela, M., "Low-Reynolds Number Airfoil Design for the MIT Daedalus Prototype: A Case Study," *Journal of Aircraft*, Vol. 25, No. 8, Aug. 1988.

AIAA 97-0054

A Hybrid Airfoil Design Method to Simulate Full-Scale Ice Accretion Throughout a Given C_l -Range

Farooq Saeed, Michael S. Selig and Michael B. Bragg
University of Illinois at Urbana-Champaign
Urbana, IL

35th Aerospace Sciences
Meeting & Exhibit
January 6-10, 1997 / Reno, NV

A HYBRID AIRFOIL DESIGN METHOD TO SIMULATE FULL-SCALE ICE ACCRETION THROUGHOUT A GIVEN C_l-RANGE

Farooq Saeed,* Michael S. Selig[†] and Michael B. Bragg[‡]

Department of Aeronautical and Astronautical Engineering
University of Illinois at Urbana-Champaign
Urbana, Illinois 61801

ABSTRACT

A design procedure for hybrid airfoils with full-scale leading edges and redesigned aft-sections that exhibit full-scale airfoil water droplet impingement characteristics throughout a given C_l-range is presented. The design procedure is an extension of the method first published by Saeed, et al., in that it not only allows for subcritical and viscous flow analysis in the design but is also capable of off-design droplet impingement simulation through the use of a flap system. The limitations of the flap-system based design for simulating both on- and off-design full-scale droplet impingement characteristics and surface velocity distribution are discussed with the help of specific design examples. In particular, the paper presents the design of two hybrid airfoils at two different angles of attack, such that they simulate both full-scale velocity distribution as well as droplet impingement at the respective design angles of attack. Both of the hybrid airfoils are half-scale airfoil models with a 5% upper and 20% lower full-scale surface of the Learjet 305 airfoil leading-edge. The effect of flap deflection and droplet size on droplet impingement characteristics is also presented to highlight the important limitations of the present method both on and off design. The paper also discusses important compromises that must be made in order to achieve full-scale ice accretion simulation throughout a desired C_l-range and suggests alternatives such as applying a multipoint design approach for the design.

NOMENCLATURE

C_l = airfoil lift coefficient
c = airfoil chord length
S = airfoil surface arc length measured from the leading-edge
T = freestream static temperature

V = surface velocity
V_∞ = freestream velocity
$\overline{V}$ = surface velocity normalized by V_∞
VMD = volume median droplet diameter
x, y = airfoil coordinates
α = angle of attack relative to the chord line
α_e = effective angle of attack relative to the nose-section chord line, $\alpha - \gamma$
β = local impingement efficiency
γ = nose droop angle
Γ = circulation strength normalized by $V_\infty c$
δ = droplet diameter
δ_f = flap deflection, deg

Subscripts:
fs = full-scale airfoil
l = lower surface
ss = subscale airfoil
u = upper surface

INTRODUCTION

Recent aircraft accidents have raised important flight safety[1-5] issues related to the operation of aircraft under severe weather conditions. To improve flight safety, a better understanding of the effect of ice accretion on the aerodynamic performance of modern airfoils is required. One important step in the process is to evaluate the aerodynamic performance of the airfoil sections, or the wing as a whole, at the icing conditions within the certification icing envelop that results in the largest performance penalties.

For aircraft safety, one of the most important performance parameters is the maximum lift coefficient. Therefore, while drag and pitching moment are important, the icing condition that results in the largest degradation in maximum lift coefficient is the most critical icing condition. The determination of the critical ice accretion and its aerodynamic effect on a set of modern airfoils, typical of those in use on aircraft, is underway at NASA Lewis Research Center. The research reported here is part of this larger effort.

Owing to the difficulties and uncertainties in ice accretion scaling,[6-14] testing at full-scale is desirable, yet costly. Moreover, available ice accretion tunnels are too small to test full-scale airfoils or wings of most aircraft of interest. One way to ex-

* Graduate Research Assistant. Student Member AIAA.
† Assistant Professor. Member AIAA.
‡ Professor. Associate Fellow AIAA.

pand the usefulness of existing icing tunnels and to facilitate testing of aircraft deicing/anti-icing systems is to test "hybrid airfoils" or "sub-scale airfoils" with full-scale leading edges and redesigned aft sections to provide full-scale icing conditions at the leading edge. The term "hybrid method" refers to using a full-scale leading edge to match the full-scale ice accretion. The aft section of the hybrid airfoil is specially designed to provide flowfield and droplet impingement similar to that on the full-scale airfoil leading-edge. One such approach[15] used airfoils with full-scale leading edges and truncated aft-sections to simulate the flowfield of the full scale, thereby avoiding the ice-accretion process on the airfoil leading edge and the associated scaling issues altogether. Interestingly, neither the approach, nor its range of application, received much attention despite its numerous merits since it permits an indepth study of droplet impingement and ice accretion on full-scale leading-edge sections within the capabilities of current icing research facilities.

In the absence of a systematic study to provide insight into the design of the aft section, a recent study[16] was carried out in which a design procedure for hybrid airfoils was successfully developed and demonstrated with specific design examples. The study showed that hybrid airfoils could be designed to exhibit both the full-scale velocity distribution on its nose section as well as full-scale droplet-impingement characteristics and, therefore, ice accretion. An inherent limitation of the design procedure outlined in the study[16] is that the method was restricted to a single-point design and, therefore, lacked the capability to handle off-design cases. Moreover, the method used the "matched lift coefficient" technique to correct for viscous effects.

To overcome these limitations, the present study was carried out with the objective to expand the scope of the single-point design procedure of Ref. 16 to a method that enables the hybrid airfoils to exhibit both full-scale velocity distribution as well as droplet impingement and, therefore, ice accretion throughout a desired C_l-range or a range of angles of attack α.

The task of simulating off-design full-scale droplet impingement, as will be shown later, is successfully accomplished by introducing a plain flap on the hybrid airfoil. The use of a plain flap, however, fails to simulate full-scale velocity distribution at the off-design conditions. Since the difference in the velocity distribution on the nose section will effect the thermodynamics of ice accretion as the droplets impinge on the surface, it therefore becomes necessary to simulate the full-scale velocity distribution in ad-

dition to droplet impingement at the off-design conditions. Thus, to simulate both the full-scale velocity distribution as well as droplet impingement on the nose section of the hybrid airfoil throughout a desired C_l-range, it is necessary to formulate a multipoint hybrid airfoil design method.

To set the stage for the multipoint design method, the paper presents the design of two half-scale hybrid airfoils that are designed at two different angles of attack such that they simulate both the full-scale velocity distribution as well as droplet impingement characteristics on the nose sections at their respective design angles of attack. The velocity distribution and droplet impingement characteristics of the two hybrid airfoils are then analyzed at an off-design angle of attack and compared with that of the full-scale airfoil. The results are then used to highlight the limitations of the present method and, therefore, suggest a need for a multipoint design method. Important compromises that must be made to achieve a multipoint design for full-scale ice accretion simulation throughout a desired C_l-range are also discussed.

DESIGN APPROACH

The hybrid airfoil design procedure for full-scale flowfield and droplet impingement simulation uses validated computational airfoil aerodynamics and droplet impingement codes,[17-32] specifically, an inverse design method,[32] the Eppler code,[25-27] XFOIL[31] and AIRDROP.[20-22] Reference 16 gives a brief discussion on each of these codes. For a more detailed discussion, the reader is referred to the associated literature.

Unlike the method presented in Ref. 16 where in the potential flow is corrected for viscous effects using the "matched lift coefficient" technique, the present method uses a modified version of XFOIL. The modified version of XFOIL was obtained by integrating the droplet-trajectory and impingement-characteristics calculation subroutines from the AIRDROP code into the XFOIL code. This was especially done to take advantage of XFOIL's ability to analyze both inviscid/viscous flow as well as incompressible/subcritical flows unlike the AIRDROP code, which is purely based on incompressible flow formulation. In this paper, the modified version of XFOIL will be referred to as the XFOIL/AIRDROP code. Once the flowfield is determined using known flight and icing conditions, the droplet trajectory calculation subroutines are then used in conjunction with the flow solver subroutines to determine the water droplet impingement on the airfoil surface.

2

A conceptual illustration of the hybrid airfoil design procedure is shown in Fig. 1. A brief summary of these steps is as follows. First, a full-scale airfoil geometry is selected and the desired flight and icing conditions are specified. In particular, the Learjet 305 airfoil (shown in Fig. 2) is used in this study to demonstrate the design procedure. The XFOIL/AIRDROP code is then used to predict the limits of droplet impingement. Once the limits of impingement are known on the leading edge of the full-scale airfoil, that part of the full-scale airfoil geometry is fixed for the subsequent hybrid airfoil shapes. As in Ref. 16, this fixed leading-edge section will be referred to as the nose section and the remaining section of the subscale airfoil profile will be referred to as the aft section. The aft section of the hybrid airfoil is then designed to provide full-scale flowfield and droplet impingement characteristics on the nose section of the hybrid airfoil.

An initial geometry for the aft section is obtained through the use of a multipoint inverse airfoil design code[32] (PROFOIL). The design of the intermediate airfoil, from which the aft section of the subscale airfoil is derived, is governed by several constraints, namely, the scale of the subscale airfoil, the upper and lower surface thickness and slope at the junction between the nose and aft sections, and a desired form for the pressure recovery characteristics. Apart from these constraints, additional continuity and closure constraints that form an integral part of the inverse design methodology[32] are also satisfied to achieve a physically realizable design. A multi-dimensional Newton iteration scheme is further employed to satisfy these constraints.

The flow over the hybrid airfoils is then analyzed using the XFOIL/AIRDROP code. In order to have a physically similar flow in the vicinity of the nose section of both the hybrid and the full-scale airfoils, the analysis is performed at the same angle of attack relative to the nose-section chord of both the airfoils. The local velocity distributions over the nose section and the stagnation point locations on both the hybrid and full-scale airfoils are then compared. If the desired velocity distribution over the nose section and stagnation point location are not achieved, the aft section of the hybrid airfoil is redesigned and again merged with the nose section to form a new hybrid airfoil. The flow over the new hybrid airfoil is then analyzed and compared with that over the full-scale airfoil. The process is repeated until the desired velocity distribution over the nose section is achieved.

In the next step, the water droplet trajectories and water droplet impingement characteristics are determined from the XFOIL/AIRDROP code. The individual droplet trajectories are combined to calculate the droplet impingement characteristics of the airfoil. The droplet impingement characteristics of both the full-scale and the hybrid airfoil are then compared. If the agreement in the droplet impingement characteristics is poor, the hybrid airfoil is modified and the design process is repeated again until good agreement is reached. At this stage, the single-point design is accomplished. To achieve off-design full-scale ice accretions or droplet impingement characteristics, a plain flap is employed on the hybrid airfoil. Thus, by deflecting the flap, the desired droplet impingement characteristics are achieved over the hybrid airfoil for the off-design cases.

The off-design cases reveal, as will be shown in the next section, certain important limitations of the design method. These limitations include 1) the onset of flow separation on the hybrid airfoils at moderate to high angles of attack conditions and 2) a mismatch in the velocity distribution on the nose section at off-design angles of attack. The former limitation can be improved either by using a more sophisticated flap system or by applying less conventional techniques such as boundary-layer control through slot suction[33,34] or circulation control via trailing-edge blowing. The latter, however, is an important limitation of the present design method and can be overcome by using a multipoint design approach.

IMPLEMENTATION

In this section, the effects of various parameters on two single-point airfoil designs are discussed. In particular, two half-scale hybrid airfoils were designed at different angles of attack such that they simulated both the full-scale velocity distribution on the nose section as well as droplet impingement characteristics at the design conditions (single-point design). The off-design full-scale velocity distribution and droplet impingement simulation characteristics of each hybrid airfoil are compared to highlight important limitations of the present method.

Single-Point Design and Simulation

The design of two half-scale models of the GLC 305 airfoil that simulate full-scale velocity distribution and droplet impingement is presented. Of the two hybrid airfoils A and B, hybrid airfoil A is designed to simulate full-scale ice accretion at $\alpha = 2$ deg while hybrid airfoil B is designed to simulate full-scale ice accretion at $\alpha = 6$ deg along with the icing conditions: $V_\infty = 90$ m/s (175 kt), $T = -10°C$, $Re = 6 \times 10^6, M = 0.28$ and $VMD = 20\mu$m. While it is realized that in flight the conditions will change

Table 1 Design flight and icing conditions.

Variable	Full scale	Hybrid A	Hybrid B
V_∞, m/s	90	90	90
T, deg C	-10	-10	-10
Re	6×10^6	3×10^6	3×10^6
M	0.28	0.28	0.28
c, m	1.0	0.5	0.5
VMD, μm	20	20	20
α, deg	2, 6	2	6
γ, deg	0	-1.5	-3
α_e, deg	2, 6	3.5	9

with angle of attack, the conditions for both angles are held constant here to simply illustrate the method.

As a first step, the droplet impingement efficiency β for the GLC 305 airfoil corresponding to the given flight and icing conditions is determined by the XFOIL/AIRDROP code. The results are shown in Fig. 3. For $\alpha = 6$ deg, the XFOIL/AIRDROP code predicts the maximum limits of impingement as $S_u = 0.0076\,(x/c = 0.0019)$ on the upper surface and $S_l = -0.1822\,(x/c = 0.1738)$ on the lower surface. Since the limits of impingement define the surface over which ice will accrete on the airfoil, only that part of the full-scale airfoil geometry needs be fixed as the nose section for the hybrid airfoil. Thus, the nose-section geometry for both the hybrid airfoils was selected as the full-scale airfoil surface from $x/c = 0.05$ on the upper surface to $x/c = 0.20$ on the lower surface. The two hybrid airfoils were then designed following the procedure illustrated in Fig. 1. Table 1 lists the flight and icing conditions for the final single-point design.

A comparison of the full-scale airfoil velocity distribution with that of the individual hybrid airfoil velocity distributions (Figs. 4a and 5a) at the single-point design conditions shows good agreement over the common nose section. Comparisons of the impingement characteristics (Figs. 4b and 5b) and tangent droplet trajectories (Figs. 4c and 5c) also indicate excellent agreement with that of the full-scale. The tangent droplet trajectories, although originating from different locations upstream are matched in the vicinity of the leading edge. This is consistent with the observations made during the case studies in Ref. 16. At this point, the single-point design for full-scale velocity distribution and droplet impingement simulation is complete and the two hybrid airfoils along with the Learjet 305 airfoil are shown in Fig. 6.

Effect of Droplet Size

The impingement characteristics, i.e., the lim-
its of impingement, the impingement efficiency β (β–curve) and the maximum point on the β–curve, referred to as β_{max}, of an airfoil depend to a large extent on the size of the water droplets in the flow. In the case of small droplets, the droplet drag dominates and the particle is very responsive to the flowfield acting almost as a flow tracer; whereas, in the case of large droplets, the droplet inertia dominates and the particle is less sensitive to changes in the flowfield. Thus, an increase in the droplet size results in an increase in the impingement efficiency β, β_{max} and the limits of impingement. It, therefore, becomes necessary to examine the effect of different droplet size on full-scale droplet impingement simulation. Since, in an actual icing cloud, the water droplets have diameters ranging from 5–50 μm, the impingement characteristics of the hybrid airfoil A were determined for two different droplet sizes. The results are presented in Fig. 7 and show good agreement where the droplet sizes are less than that selected for the single point design. For larger droplet size, a good overall agreement can be seen, however, the limits of impingement and β_{max} differ slightly.

Off-Design Simulation

To simulate full-scale ice accretion or droplet impingement characteristics throughout a desired C_l– or α–range, a flap system was employed on each of the hybrid airfoils. The objective was to match both the velocity distribution as well as the droplet impingement characteristics at any off-design angle of attack by an appropriate amount of flap deflection. To accomplish this task, the two hybrid airfoils were analyzed at off-design angles of attack, in partcular, the hybrid airfoil A designed to simulate conditions at $\alpha = 2$ deg was analyzed at $\alpha = 6$ deg while the hybrid airfoil B designed to simulate conditions at $\alpha = 6$ deg was analyzed at $\alpha = 2$ deg. The results are shown in Figs. 8 and 9 in which the hybrid airfoil velocity distribution and impingement characteristics are shown with and without the appropriate flap deflection necessary to simulate full-scale droplet impingement. The results show that, although the use of a flap on hybrid airfoils can be very effective in simulating full-scale droplet impingement characteristics at an off-design condition, it is, however, not able to accurately simulate full-scale velocity distribution over the nose section of that hybrid airfoil.

To determine the optimum flap setting, the root-mean-squares difference in local impingement efficiency RMS_β and in normalized surface velocity $RMS_{\overline{V}}$ were calculated for different angle of attack and flap settings. Mathematically, RMS_β and $RMS_{\overline{V}}$ are defined as

4

$$RMS_\beta = ||\beta_{fs}(S) - \beta_{ss}(S)|| \qquad (1)$$

$$RMS_{\overline{V}} = ||\overline{V}_{fs}(S) - \overline{V}_{ss}(S)|| \qquad (2)$$

where $S_l \leq S \leq S_u$.

Figures 10a,b show the variation in RMS_β and $RMS_{\overline{V}}$, respectively, for different angles of attack and flap settings δ_f for the hybrid airfoil A designed for $\alpha = 2$ deg while Figs. 11a,b show similar plots for the hybrid airfoil B designed for $\alpha = 6$ deg. The optimum flap deflection was then selected as the one that corresponds to the minimum value of RMS_β.

The optimum flap settings corresponding to each angle-of-attack case are plotted in Fig. 12a for clarity. Figure 12b, on the other hand, shows a comparison of the circulation Γ of both the hybrid airfoils with that of the full-scale. The results indicate that the hybrid airfoils require less circulation than the full-scale airfoil to simulate full-scale droplet impingement and that the difference between the full-scale and hybrid airfoil circulation is nearly constant until significant flow separation occurs on the hybrid airfoils. Beyond this point, the hybrid airfoil circulation starts to fall off gradually and, therefore, suggests the limit to which a hybrid airfoil can be used to simulate full-scale droplet impingement characteristics.

It is important to note in Figs. 10 and 11 that the $RMS_{\overline{V}}$ values are an order of magnitude higher than the corresponding RMS_β. Although contributions to the RMS values due to numerical noise cannot be ruled out completely, differences in surface velocity will certainly effect the thermodynamics of ice accretion. Thus, it becomes necessary to incorporate the ice accretion process in the design method in addition to flow and droplet impingement analysis.

The effect of larger droplet size on off-design simulation is shown in Fig. 13. Similar trends can be observed as in the on-design case. Since large sized droplets result in an increase in the limits of impingement, they together with the angle of attack of interest may dictate the size of the nose section and, thus, limit the range of application of the present method.

CONCLUSIONS

Several important conclusions can be drawn from this study. First, it is shown that it is possible to design hybrid airfoils with full-scale leading edges and redesigned aft-sections that exhibit full-scale airfoil water droplet impingement characteristics throughout a given C_l-range. The results indicate the usefulness of a flap system in simulating off-design full-scale droplet impingement characteristics. The use of flap for full-scale droplet impingement simulation is, however, restricted to low and moderate angles of attack since at high absolute angles of attack together with high flap deflections, the hybrid airfoils become susceptible to flow separation. This limitation can, however, be overcome by the use of a more sophisticated flap system or by the application of boundary-layer control methods.

The results of off-design simulation also reveal the existance of small differences in surface velocity distribution within the limits of droplet impingement. Since this difference in surface velocity will affect the thermodynamics of ice accretion and prevent full-scale ice accretion simulation, the present method should be modified to include the effects of ice accretion as well into the design of hybrid airfoils.

ACKNOWLEDGMENTS

REFERENCES

[1] Anon., "Selected Bibliography of NACA–NASA Aircraft Icing Publications," NASA TM 81651, Aug. 1981.

[2] Anon., "Icing Technology Bibliography," SAE AIR-4015, Warrendale, PA, Nov. 1987.

[3] Anon., "Aircraft Icing," NASA CP-2086 (FAA-RD-78-109), 1979.

[4] Brun, R. J., "Icing Problems and Recommended Solutions," AGARDograph 16, Nov. 1957.

[5] Perkins, P., and Rieke, W., "Aircraft Icing Problems — After 50 Years," AIAA Paper 93-0392, Jan. 1993.

[6] Hauger, H. H. and Englar, K. G., "Analysis of Model Testing in an Icing Wind Tunnel," Douglas Aircraft Co., Inc., Rep. No. SM 14993, May 1954.

[7] Sibley, P. J. and Smith, R. E., Jr. "Model Testing in an Icing Wind Tunnel," Lockheed Aircraft Corp., Inc., Rep. No. LR 10981, Oct. 14, 1955.

[8] Dodson, E. D., "Scale Model Analogy for Icing Tunnel Testing," Boeing Airplane Company, Transport Division, Document No. D66-7976, Mar. 1962.

[9] Bragg, M. B., Gregorek, G. M., and Shaw, R. J., "An Analytical Approach to Airfoil Icing," AIAA Paper 81-0403, Jan. 1981.

[10] Bragg, M. B., "Effect of Geometry on Airfoil Icing Characteristics," *Journal of Aircraft*, Vol. 21, No. 7, 1984, pp. 505–511.

[11] Ruff, G. A., "Verification and Application of

the Icing Scaling Equations," AIAA Paper 86-0481, Jan. 1986.

[12]Bilanin, A. J., "Proposed Modifications to Ice Accretion/Icing Scaling Theory," AIAA Paper 88-0203, Jan. 1988.

[13]Anderson, D. N., "Rime-, Mixed- and Glaze-Ice Evaluations of Three Scaling Laws," AIAA Paper 94-0718, Jan. 1994.

[14]Anderson, D. N., "Methods for Scaling Icing Test Conditions," AIAA Paper 95-0540, Jan. 1995. Also published as NASA TM 106827.

[15]Glahn, U. H. von, "Use of Truncated Flapped Airfoils for Impingement and Icing Tests of Full-Scale Leading-Edge Sections," NACA RM E56E11, Jul. 1956.

[16]Saeed, F., Selig, M. S.,and Bragg, M. B., "A Design Procedure for Subscale Airfoils with Full Scale Leading-Edges for Ice Accretion Testing," AIAA Paper 96-0635, Jan. 1996.

[17]Taylor, G. I., "Notes on Possible Equipment and Technique for Experiments on Icing on Aircraft," Aeronautical Research Council, R&M 2024, Jan. 1940.

[18]Glauert, M., "A Method of Constructing the Paths of Raindrops of Different Diameters Moving in the Neighbourhood of (1) a Circular Cylinder, (2) an Aerofoil Placed in a Uniform Stream of Air; and a Determination of the Rate of Deposit of the Drops on the Surface and the Percentage of Drops Caught," Aeronautical Research Council, R&M 2025, Nov. 1940.

[19]Langmuir, I. and Blodgett, K. B., "A Mathematical Investigation of Water Droplet Trajectories," Army Air Forces TR 5418, Feb. 1946 (Contract No. W-33-038-ac-9151 with General Electric Co.). Also available from the Department of Commerce Publication Board as PB No. 27565.

[20]Bragg, M. B., "A Similarity Analysis of the Droplet Trajectory Equation," *AIAA Journal*, Vol. 20, No. 12, 1982, pp. 1681–1686.

[21]Bragg, M. B., "AIRDROP: Airfoil Droplet Impingement Code," to be published, NASA CR.

[22]Bragg, M. B., and Gregorek, G. M., "An Incompressible Droplet Impingement Analysis of Thirty Low and Medium Speed Airfoils," The Ohio State University, Aeronautical and Astronautical Research Laboratory, TR AARL 82-02, Columbus, Ohio, Feb. 1982.

[23]Gent, R. W., "Calculation of Water Droplet Trajectories About an Aerofoil in Steady, Two-Dimensional, Compressible Flow," Royal Aircraft Establishment (RAE) TR 84060, June 1984.

[24]Theodoreson, T., and Garrick, I. E., "General Potential Theory of Arbitrary Wing Sections,"

NACA Report 452.

[25]Eppler, R., "Direct Calculation of Airfoils from Pressure Distribution," NASA TT F-15, 417, Mar. 1974. (Translated from *Ingenieur-Archive*, Vol. 25, No. 1, 1957, pp. 32–57.)

[26]Eppler, R., and Somers, Dan M., "A Computer Program for the Design and Analysis of Low-Speed Airfoils," NASA TM-80210, Aug. 1980.

[27]Eppler, R., *Airfoil Design and Data*, Springer-Verlag, New York, 1990.

[28]Woan, C. J., "Fortran Programs for Calculating the Incompressible Potential Flow About a Single Element Airfoil Using Conformal Mapping," The Ohio State University, Aeronautical and Astronautical Research Laboratory, TR AARL 80-02, Columbus, Ohio, Jan. 1980.

[29]Drela, M., and Giles, M. B., "ISES: A Two-Dimensional Viscous Aerodynamic Design and Analysis Code," AIAA 87-0424, Jan. 1987.

[30]Drela, M., "Low-Reynolds Number Airfoil Design for the MIT Daedalus Prototype: A Case Study," *Journal of Aircraft*, Vol. 25, No. 8, Aug. 1988.

[31]Drela, M., "XFOIL: An Analysis and Design System for Low Reynolds Number Airfoils," *Lecture Notes in Engineering: Low Reynolds Number Aerodynamics*, T. J. Mueller (ed.), Vol. 54, Springer-Verlag, New York, June 1989, pp. 1–12.

[32]Selig, M. S., and Maughmer, M. D., "A Multipoint Inverse Airfoil Design Method Based on Conformal Mapping," *AIAA Journal*, Vol. 30, No. 5, 1992, pp. 1162–1170.

[33]Saeed, F., and Selig, M. S., "A Multipoint Inverse Design of Airfoils with Slot-Suction ," *Journal of Aircraft*, Vol. 33, No. 5, 1996, pp. 708–715.

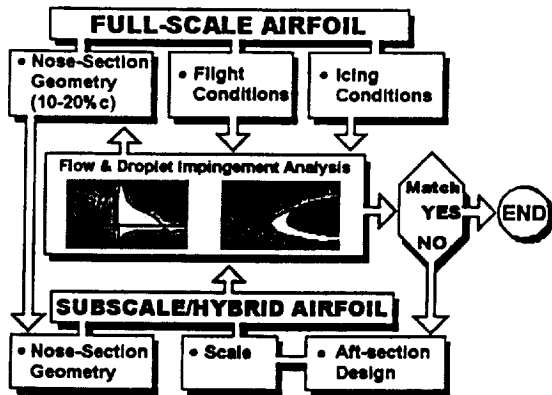[34]Saeed, F., and Selig, M. S, "A New Class of Airfoils Using Slot-Suction," AIAA Paper 96-0058, Jan. 1996.

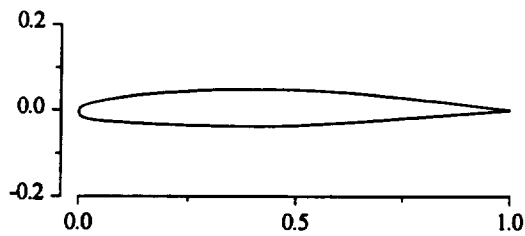Fig. 1 The subscale/hybrid airfoil design procedure.

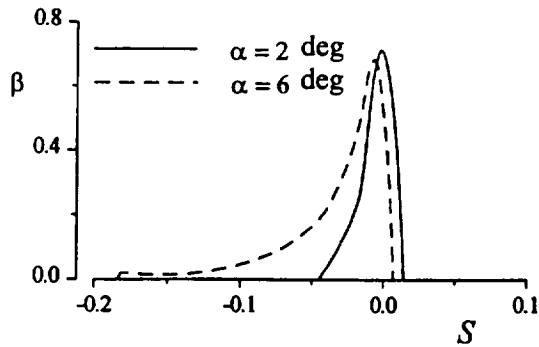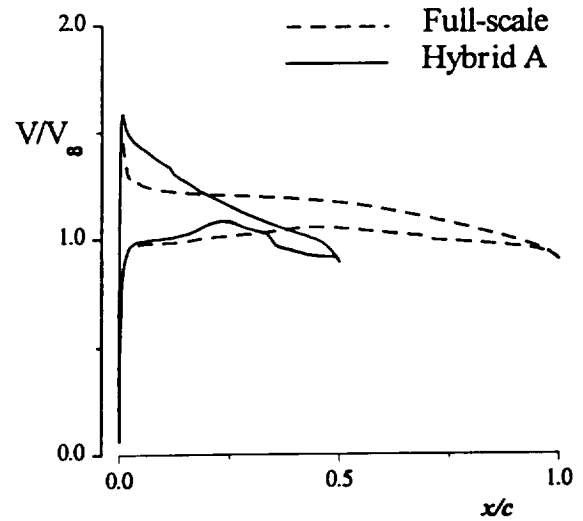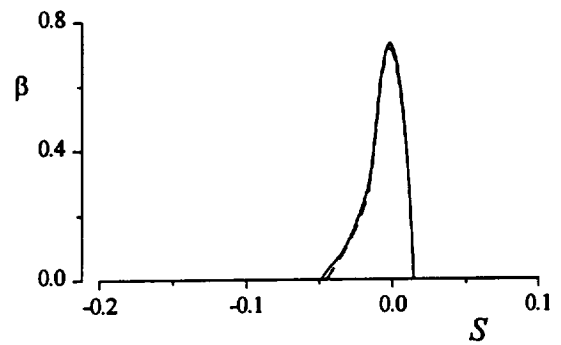Fig. 2 Learjet 305 (GLC 305) airfoil.

Fig. 3 Droplet impingement efficiency for the Learjet 305 airfoil.
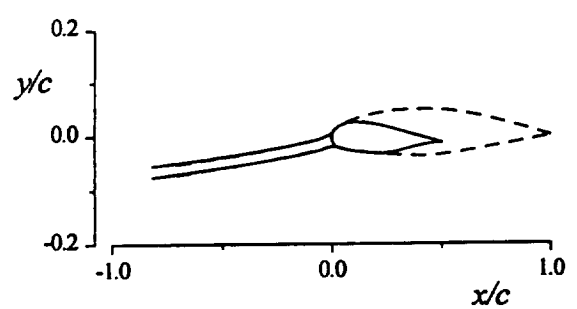
(a)

(b)

(c)

Fig. 4 Comparison of full-scale and hybrid airfoil A (a) velocity distributions, (b) droplet impingement efficiencies and (c) tangent droplet trajectories at the design angle of attack $\alpha = 2$ deg.
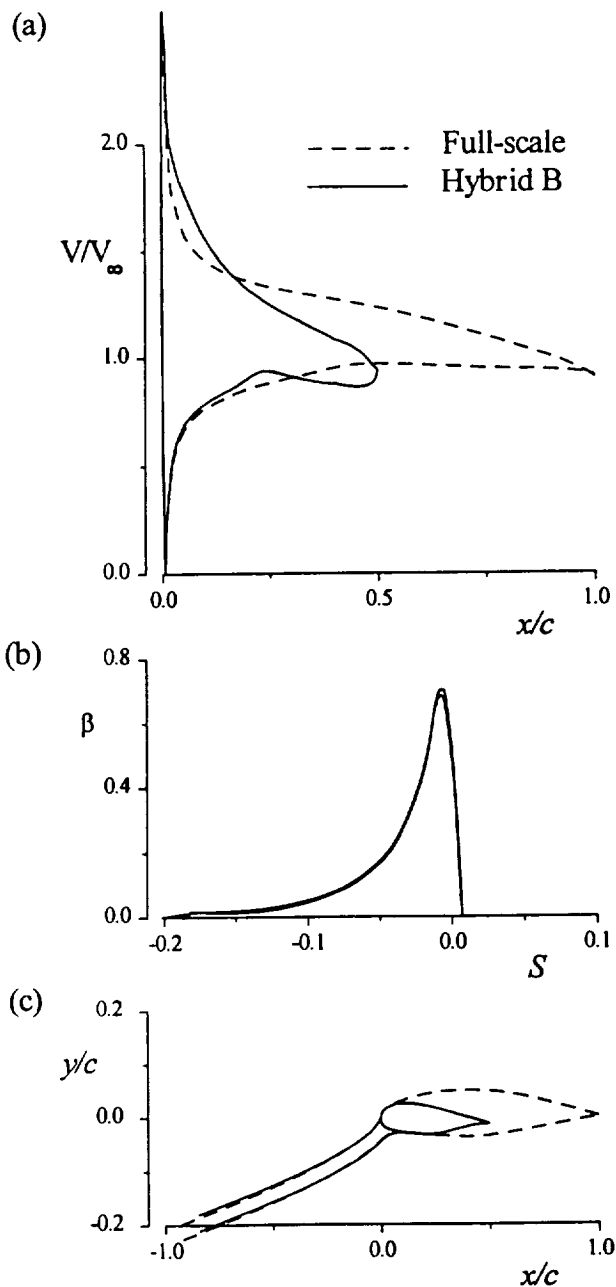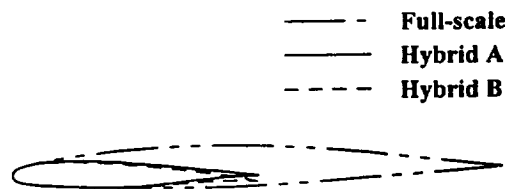
7

(a)

V/V∞

- - - - Full-scale
——— Hybrid B

(b) β

(c) y/c

- - - Full-scale
——— Hybrid A
- - - - Hybrid B

Fig. 6 The two hybrid airfoils and the Learjet 305 airfoil.

(a) β

- - - - Full-scale
——— Hybrid A

(b) β

Fig. 5 Comparison of full-scale and hybrid airfoil B (a) velocity distributions, (b) droplet impingement efficiencies and (c) tangent droplet trajectories at the design angle of attack $\alpha = 6$ deg.
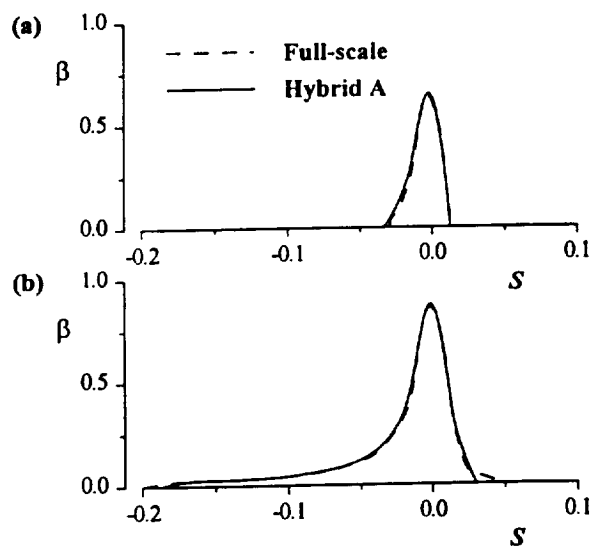
Fig. 7 Comparison of full-scale and hybrid airfoil A droplet impingement efficiencies for (a) 5 micron and (b) 40 micron droplet size at the design angle of attack.
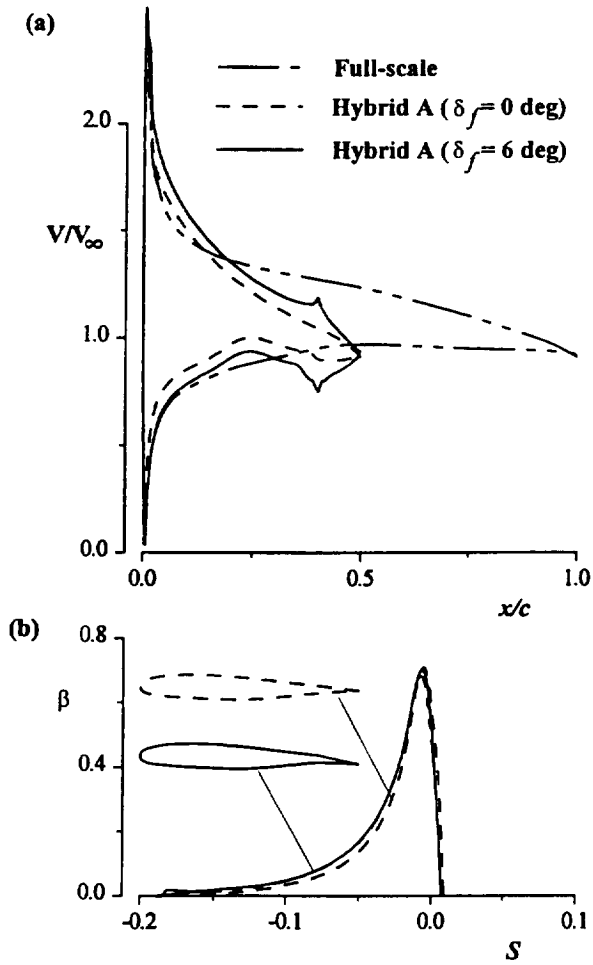
8

Fig. 8 Comparison of full-scale and hybrid airfoil A (a) velocity distributions and (b) droplet impingement efficiencies at off-design angle of attack $\alpha = 6$ deg with and without flap deflection.

Fig. 9 Comparison of full-scale and hybrid airfoil B (a) velocity distributions and (b) droplet impingement efficiencies at off-design angle of attack $\alpha = 2$ deg with and without flap deflection.
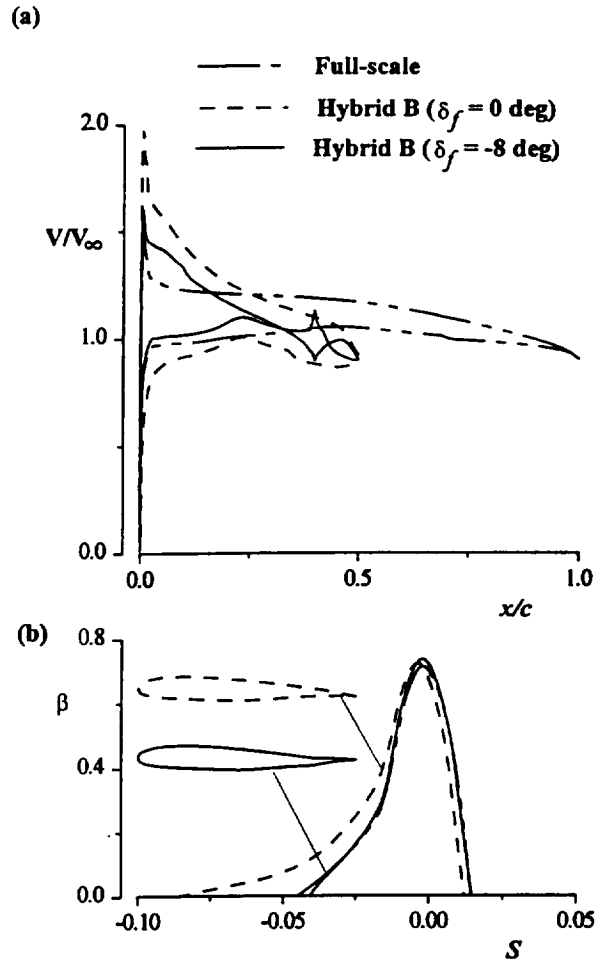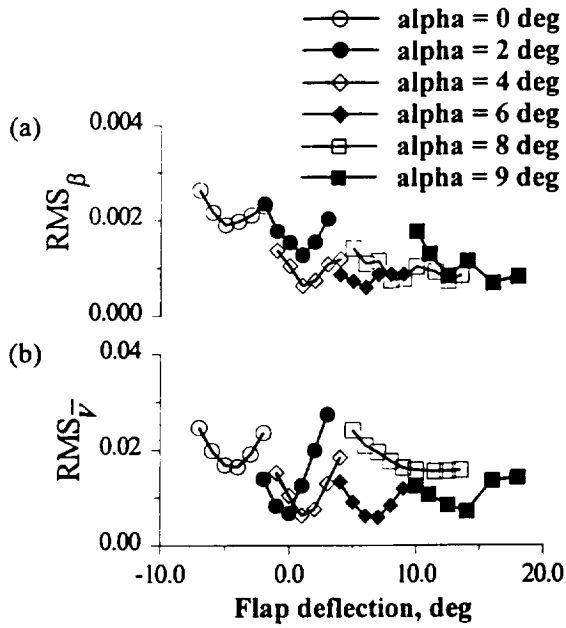
(a)

- alpha = 0 deg
- alpha = 2 deg
- alpha = 4 deg
- alpha = 6 deg
- alpha = 8 deg
- alpha = 9 deg

RMS_β 0.004

0.002

0.000

(b) $RMS_{\bar{V}}$ 0.04

0.02

0.00

-10.0   0.0   10.0   20.0

Flap deflection, deg

Fig. 10 The variation in the RMS values for different angles of attack and flap settings for the hybrid airfoil A.

(a) RMS_β 0.004

0.002

0.000

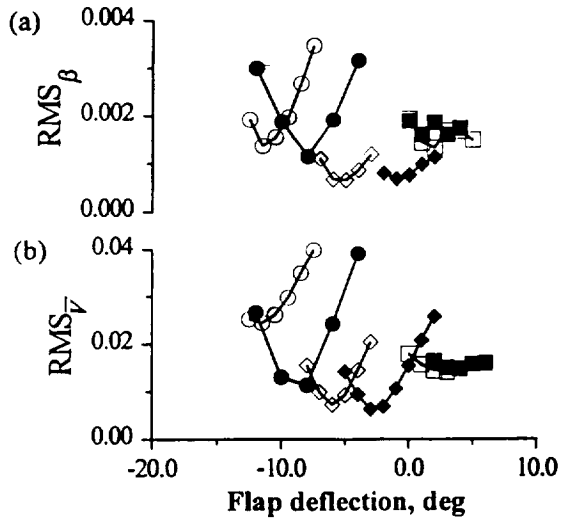(b) $RMS_{\bar{V}}$ 0.04

0.02

0.00

-20.0   -10.0   0.0   10.0

Flap deflection, deg

Fig. 11 The variation in the RMS values for different angles of attack and flap settings for the hybrid airfoil B.

(a) Flap deflection, deg
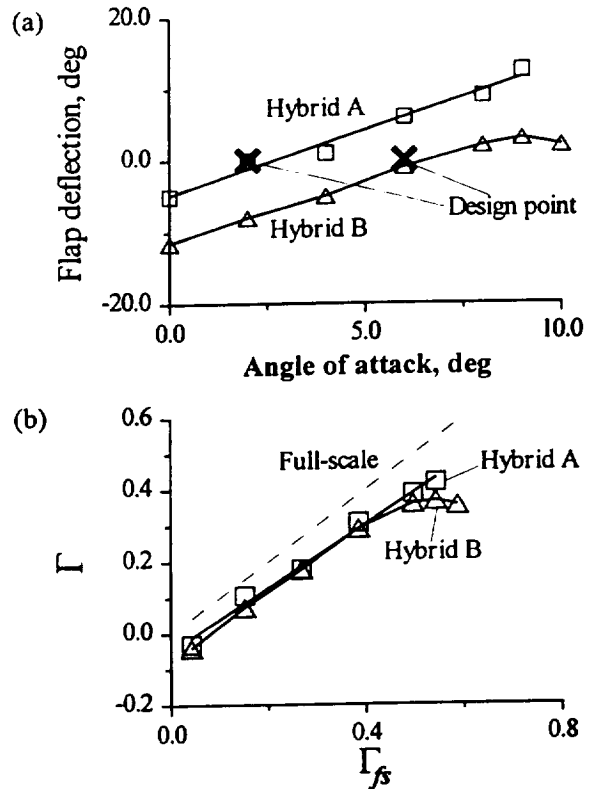
20.0

Hybrid A

0.0

Design point

Hybrid B

-20.0

0.0   5.0   10.0

Angle of attack, deg

(b) Γ 0.6

Full-scale   Hybrid A

0.4

0.2

Hybrid B

0.0

-0.2

0.0   0.4   0.8

Γ_{fs}

Fig. 12 Plot of (a) the optimum flap deflection and (b) the respective airfoil circulation.

β 1.0

- - - - Full-scale

Hybrid B

0.5

0.0
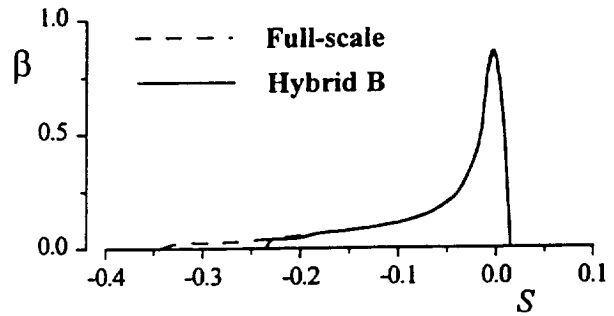
-0.4   -0.3   -0.2   -0.1   0.0   0.1

S

Fig. 13 Comparison of off-design droplet impingement efficiency for 40 micron droplet size at α = 4 deg.